Isospin equilibration in multinucleon transfer reaction at near-barrier energies

Cheng Li [1,2],[*] Cheikh A.T. Sokhna [1,2], Xinxin Xu [1,2], Jingjing Li [1,2],
Gen Zhang [1,2], Bing Li [1,2], Zhishuai Ge [1,2], and Feng-Shou Zhang [1,2,3][†]

[1] *Beijing Radiation Center, Beijing 100875, China*
[2] *College of Nuclear Science and Technology, Beijing Normal University, Beijing 100875, China*
[3] *Center of Theoretical Nuclear Physics, National Laboratory of Heavy Ion Accelerator of Lanzhou, Lanzhou 730000, China*

The isospin equilibration process in multinucleon transfer reactions is investigated by using the improved quantum molecular dynamics model. The collisions of ^{124}Xe+^{208}Pb at near-barrier energy are studied with different symmetry energy coefficients. We find that the neutron transfer is enhanced at the early stages of the collisions under the strong symmetry potential. The neutrons transfer takes place at earlier stage than protons. The trajectory of neutron flow is along the low-density path from the target to projectile. The average N/Z values of the primary products in ^{58}Ni+^{208}Pb reaction are also investigated and compared with available experimental data. It shows that the average N/Z values of the projectile-like products increase rapidly with increasing mass transfer. In the quasi-elastic collisions, the isospin equilibration process is incomplete due to a short contact time between the reaction partners. The complete isospin equilibration events take place in symmetric quasi-fission reactions.

I. INTRODUCTION

The isospin transport effects in heavy-ion collisions have been studied for many years[1–9]. It includes two different facets, named isospin diffusion and drift. The isospin diffusion is related to the isospin asymmetry of a system in which the projectile and target have different N/Z values [10]. The isospin drift is related to the density gradient which is expected to exist in the low-density neck region, even between two identical nuclei [11]. In the nuclear reactions, the isospin transport is initiated and continues until the system disintegrates or the chemical potentials for neutrons and protons in both nuclei become equal. If the interaction time between the projectile and target is long enough, the system will reach the situation of isospin equilibration.

In heavy-ion collisions at intermediate energies, the isospin transport effects have been investigated in mid-peripheral collisions by analyzing the N/Z values of the reconstructed primary quasi-projectile, quasi-target, and midvelocity sources. Such as in the ^{40}Ca+^{48}Ca reaction [3], one sees that the isospin diffusion effects lead to an increase of the N/Z of the quasi-projectile source. In the collisions of two identical N/Z values nuclei (such as ^{58}Ni+^{58}Ni [11]), it allows us to observe the isospin drift phenomenon without contamination from the midvelocity source.

At low incident energies, the multinucleon transfer (MNT) reaction is one of the most important mechanism, which has attracted widespread interests in recent years both experimentally [12–22] and theoretically [23–35]. Unlike at the intermediate incident energies, the collisions between the reaction partners are not violent. The major products in MNT reactions only contain the

quasi-projectlie and the quasi-target fragments with the number of nucleon transfers up to 30 or more. No midvelocity fragments are formed. In general, the MNT reactions include the quasi-elastic, the deep-inelastic, and the quasi-fission reactions. These reaction mechanisms can be distinguished by analyzing the total-kinetic-energy-mass (TKE-Mass) distributions combined with the total kinetic energy loss (TKEL) distributions of the products [36–38]. The contact times between the reaction partners for the quasi-elastic, the deep-inelastic, and the quasi-fission reactions are quite different. The MNT reactions provide an opportunity to study the isospin equilibration process under the different time scales. In the quasi-fission reactions, the typical time scales can reach 10^{-21} s order of magnitude or longer [39, 40]. In this case, the nucleon transfer process may lead to a uniform distribution of the N/Z ratio.

Many experiments about the isospin equilibration effects at low-energies have been performed by analyzing the N/Z values of reconstructed primary products during the last decades [18, 41–43]. For example, the reactions of ^{64}Ni+^{130}Te at E_{lab} = 275 MeV and ^{58}Ni+^{208}Pb at E_{lab} = 345 MeV have been investigated by Królas et al. at Laboratori Nazionali di Legnaro (INFN) [18]. It is found that the isospin equilibration process is closely related to the number of nucleon transfer between the reaction partners. Actually, it is difficult to divide the contributions of the isospin diffusion and drift at low-energies separately. The isospin equilibration is one important mechanism in the MNT reactions, which is one promising approach to produce new neutron-rich nuclei. For example, the new isotopes ^{54}Ti, ^{56}V, ^{58,59}Cr, ^{61}Mn, and ^{63,64}Fe were produced by Guerreau et al. through a 340 MeV ^{40}Ar beam accelerated by the Orsay ALICE accelerator facility bombarding on ^{238}U target [44].

The neck is an important characteristic in MNT reactions, even in the early stage of the fusion reaction. It is formed in the dinuclear system and is characterized by sub-saturation densities. The isospin transport

[*] licheng@mail.bnu.edu.cn
[†] Corresponding author: fszhang@bnu.edu.cn

and the energy dissipation processes of the system are closely related to the nucleon transfer between the reaction partners through the neck. The dynamical calculation is required to understand some details of these processes. A microscopic dynamics model, the improved quantum molecular dynamics (ImQMD) model [45, 46], describe the nuclear reactions based on effective nucleon-nucleon interaction. The ImQMD model is self-consistent for describing the behavior of neck evolution and nucleon transport during the collisions. In this work, we apply the ImQMD model to investigate the isospin equilibration process in the reactions of ^{124}Xe+^{208}Pb and ^{58}Ni+^{208}Pb at near-barrier energies.

The structure of this paper is as follows. In Sec. II, we briefly introduce the ImQMD model. The results and discussion are presented in Sec. III. Finally, the conclusion is given in Sec. IV.

II. THE MODEL

The ImQMD model is an improved version of the quantum molecular dynamics (QMD) model [47]. The standard Skyrme interaction with the omission of the spin-orbit term is adopted for describing the bulk and surface properties of nuclei [45]. The stochastic two-body collision process is added to the time evolution by the Hamilton equation of motion. To describe the fermionic nature of the N-body system, the Fermi constraint proposed by Papa et al. in the constrained molecular dynamics (CoMD) model [48, 49] is introduced. It improves greatly the stability of an individual nucleus. The final state of the two-body collision process is checked so that it obeys the Pauli principle. The detailed descriptions of the ImQMD model can be found in Refs. [45, 46]. The nuclear interaction potential can be read as

$$V_{\mathbf{loc}} = \frac{\alpha}{2}\frac{\rho^2}{\rho_0} + \frac{\beta}{\gamma+1}\frac{\rho^{\gamma+1}}{\rho_0^\gamma} + \frac{g_{sur}}{2\rho_0}(\nabla\rho)^2$$
$$+ \frac{C_s}{2\rho_0}(\rho^2 - \kappa_s(\nabla\rho)^2)\delta^2 + g_\tau\frac{\rho^{\eta+1}}{\rho_0^\eta}. \quad (1)$$

Here $\rho = \rho_n + \rho_p$ is the nucleons density. $\delta = (\rho_n - \rho_p)/(\rho_n + \rho_p)$ is the isospin asymmetry. The first three terms in above expression are obtained from the potential energy functional of Skyrme interaction directly. The fourth term is the symmetry potential energy including the bulk and the surface symmetry potential energies. The surface symmetry potential energy term is related to the density gradient which is important for describing the neutron skin of nuclei. The last term is a small correction term. The density distribution function ρ of a system can be read

$$\rho(r) = \sum_i \frac{1}{(2\pi\sigma_r^2)^{3/2}}\exp[-\frac{(\boldsymbol{r}-\boldsymbol{r}_i)^2}{2\sigma_r^2}]. \quad (2)$$

σ_r is the wave-packet width of the nucleon in coordinate space. The IQ2 parameter sets (see Table 1) adopted in

this work are the same as in Refs. [24, 32]. The incompressibility coefficient, K_∞, is 195 MeV. This parameter sets have been successfully applied on the heavy-ion collisions in fusion reactions [46, 50], multinucleon transfer reactions [24, 32], and ternary breakup reactions[51].

TABLE I. The model parameters (IQ2) adopted in this work.

α (MeV)	β (MeV)	γ	g_{sur} (MeV fm^2)	g_τ (MeV)	η	C_S (MeV)	κ_s (fm^2)	ρ_0 (fm^{-3})
-356	303	7/6	7.0	12.5	2/3	32.0	0.08	0.165

In this work, we set z-axis as the beam direction and x-axis as the impact parameter direction. We set the wave-packet width $\sigma_r = 1.3$ fm to calculate the isospin equilibration process of ^{124}Xe+^{208}Pb and ^{58}Ni+^{208}Pb. The initial distance of the center of mass between the projectile and target is 30 fm.

III. RESULTS AND DISCUSSION

We first test the ImQMD model for the description of the MNT reactions. The collisions of ^{58}Ni+^{208}Pb at $E_{\mathrm{lab}} = 328.4$ MeV are simulated by using the ImQMD model. 39000 simulation events are calculated with the impact parameters from 0 to $b_{\max}$ fm. $b_{\max} = R_{\mathrm{P}} + R_{\mathrm{T}}$, where R_{P} and R_{T} denote the radius of the projectile and the target, respectively. For each event, we simulate the collision process until $t = 2000$ fm/c with a step size of $\Delta t = 1$ fm/c. Figure 1 shows the isotope production cross sections from Mn to Ni. The fusion and elastic scattering events are not taken into account. The experimental data are taken from Ref. [52]. The thick folding lines and thick solid lines denote the calculations from the combination of ImQMD+GEMINI and GRAZING model [53–55] with inclusion of the evaporation, respectively. The nuclear level densities in the GEMINI code [56] are taken as a Fermi-gas form with the default parameters. From Fig. 1 we find that the measured isotope distributions for the elements Co and Ni can be reasonably well reproduced by the ImQMD+GEMINI calculations. The discrepancy between the data and the calculations increases with the increasing number of proton transfer. The GRAZING calculations also show a similar behavior.

For simplicity, we consider head-on collisions of ^{124}Xe+^{208}Pb at $E_{\mathrm{c.m.}} = 450$ MeV to investigate the isospin equilibration process. For this reaction, the incident energy is slightly higher than the Coulomb barrier. It is almost impossible to form a compound nucleus, due to large $Z_{\mathrm{P}}Z_{\mathrm{T}}$ value. The typical reaction process is that the colliding nuclei exchange a number of nucleons and then re-separate. Figure 2 shows the single-particle potentials of neutrons and protons in ^{124}Xe+^{208}Pb along the beam direction at $t = 200$ and 300 fm/c. The single-particle potential is defined as $V_{sp}^q(\mathbf{r}) = \int \rho(\mathbf{r}')V(\mathbf{r} - \mathbf{r}')d\mathbf{r}'$, where $q = n, p$, $\rho(\mathbf{r})$ is the density distribution of the system, and $V(\mathbf{r} - \mathbf{r}')$ is the effective nucleon-nucleon interaction. The Coulomb
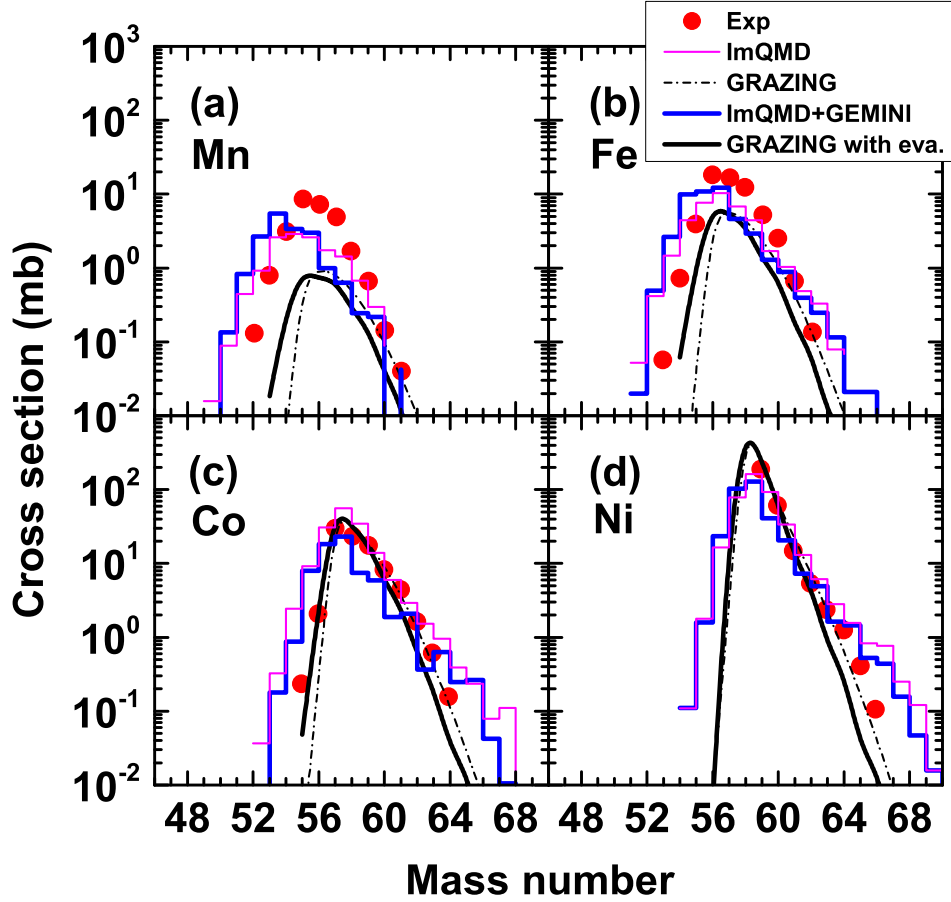
FIG. 1. (Color online.) Isotope production cross sections from Mn to Ni in the reaction of ^{58}Ni+^{208}Pb at $E_{\mathrm{lab}} = 328.4$ MeV. The thick folding lines and thick solid lines denote the calculations from the combination of ImQMD+GEMINI and GRAZING model with inclusion of the evaporation, respectively. The thin folding lines and thin dash-dotted lines denote the primary fragment distributions from the ImQMD and GRAZING models, respectively. The experimental data (solid circles) are taken from Ref. [52].

interaction is very important for the isospin transport processes in the early stage of the MNT reactions. For example, at $t = 200$ fm/c, the neutron transfer is allowed due to lower barrier between the two reaction partners (see Fig. 2(a)). However, for protons, the proton transfer between two reaction partners is forbidden at this time because the barrier is very high (see Fig. 2(c)). Hence, the neutrons transfer process takes place at earlier stage than the protons in the MNT reactions. At $t = 300$ fm/c, the barriers between the reaction partners are reduced both for neutrons and protons. Therefore, both the neutrons and protons are allowed to transfer between the target and projectile (see Fig. 2(b) and 2(d)).

Figure 3 shows the time evolution of the density profiles for ^{124}Xe+^{208}Pb at $E_{\mathrm{c.m.}} = 450$ MeV. As seen from the figure, the central densities of nuclei in the reactions are reasonable. In addition, we note that the diffuse-ness of density can be seen clearly on the surface of the system. In Fig. 4, we show the contour plots of isospin asymmetry ($\delta = (\rho_n - \rho_p)/(\rho_n + \rho_p)$) for the ^{124}Xe+^{208}Pb during the evolution of the system. The average values of isospin asymmetry for ^{124}Xe and ^{208}Pb nuclei are 0.13 and 0.21, respectively. From Fig. 4, one sees that the distributions of the isospin asymmetry in the cores of two reaction partners are uniform. The corresponding values of δ in the quasi-projectile and quasi-target are 0.1 and 0.17, respectively. However, the values of isospin asymmetry on the surface of the nuclei are significantly larger than those in cores. The core of ^{208}Pb is covered by neutron skin with maximal $\delta = 0.54$ at $t = 50$ fm/c. The neutron enrichment can also be seen clearly in the low-density neck region. This phenomenon is known as the isospin drift which is due to the density gradient. The neutrons are preferably driven to the low density area
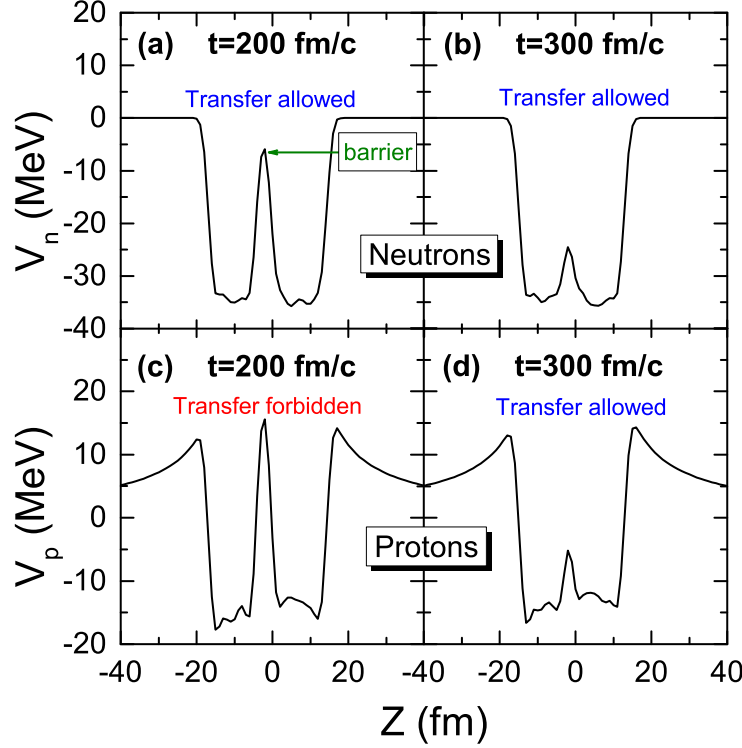
FIG. 2. (Color online.) The single-particle potentials of neutrons (up panels) and protons (bottom panels) in ^{124}Xe+^{208}Pb at $t = 200$ and $t = 300$ fm/c.

[57]. In Fig. 4, one also can see that the neutron flow in the reactions is formed along the low-density path.

In order to investigate the isospin transport during the evolution of the dinuclear system, we introduce the separation plane to divide the quasi-projectile and quasi-target nuclei. The separation plane can be defined as the plane at the position where iso-contours of the projectile and target densities cross each other. This method was adopted by the TDHF calculations in Refs. [58, 59]. Figure 5 shows the transfer coefficients of neutron and proton in the head-on collisions of ^{124}Xe+^{208}Pb with the symmetry energy coefficients of $C_s = 28$ and 32 MeV. The transfer coefficient can be read as $v_{n,p} = \mathrm{d}N_{n,p}/\mathrm{d}t$, where $N_{n,p}$ denotes the net neutron or proton flux through the separation plane. The direction of nucleon transfer is from the target to projectile. One can see that the neutron transfer is enhanced in the case of $C_s = 32$ MeV at the early stages of the collisions due to the strong symmetry potential. The corresponding peak value of the neutron transfer coefficient is about 1×10^{-2} per fm/c which is close to the TDHF calculations in Ref. [60]. The proton transfer coefficients are not sensitive to the symmetry energy in ^{124}Xe+^{208}Pb reactions. Because the symmetry energy mainly influence the neutron transport in the case that projectile and target have large

difference of N/Z values. In addition, we note that the time of neutron transfer starts at $t = 150$ fm/c which is earlier than that of proton transfer. This is due to that the proton transfer is prevented by a high barrier between the reaction partners at the early stages of the collisions (see Fig. 2(a) and 2(c)).

In MNT reactions, the contact time between the reaction partners is related to collision mode. Different collision mechanisms can be distinguished by analyzing the TKE-Mass distribution combined with the TKEL distribution of the products. In Fig. 6, we show the TKE-Mass distributions and corresponding TKEL distributions of primary binary fragments in ^{58}Ni+^{208}Pb at $E_{\mathrm{lab}} = 345$ MeV for the contact time ranges of $0 < t_{\mathrm{con}} \leq 400$, $400 < t_{\mathrm{con}} \leq 1000$, and $0 < t_{\mathrm{con}} \leq 1000$ fm/c. The contour plots show the counts of the fragments in logarithmic scale. The region of the impact parameters in calculations is from 0 to b_{max} fm. The quasi-elastic and the deep-inelastic collisions occur when the contact time is less than 400 fm/c. As shown in Fig. 6 (b), the quasi-elastic collision events can be extracted through fitting the peak of TKEL distribution by a Gaussian curve. In general, the contact time between the reaction partners for the quasi-elastic collision events is shorter than that for the deep-inelastic collision events. There are only
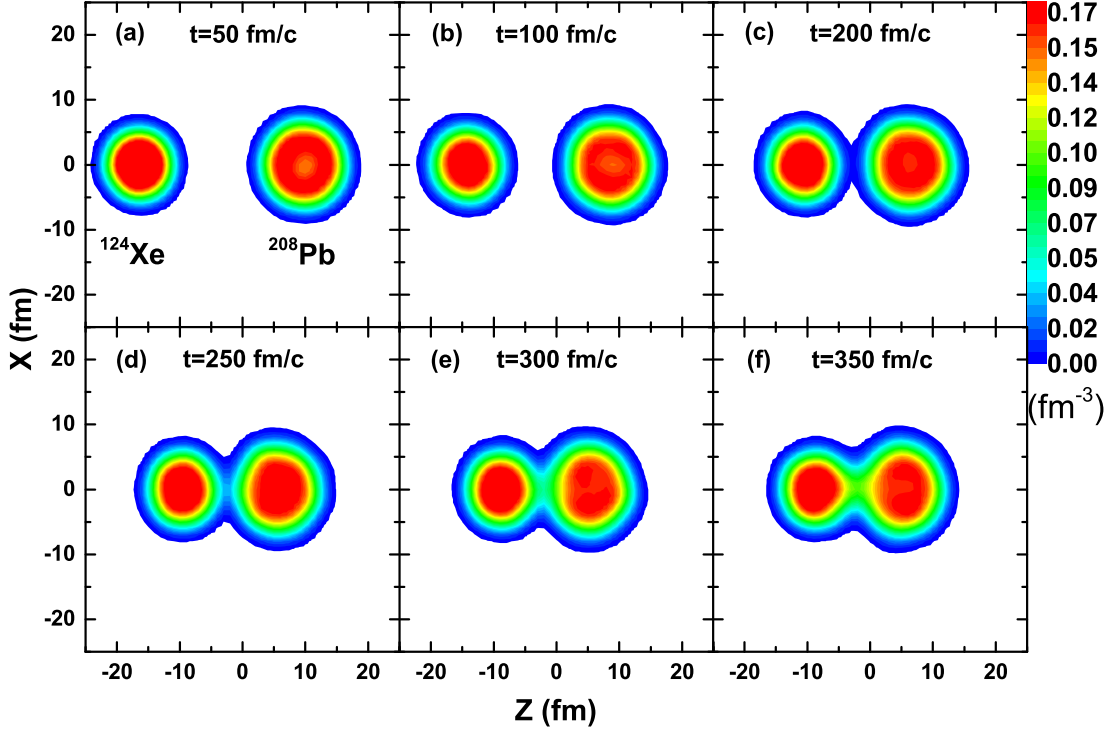
FIG. 3. (Color online.) Time evolution of the density profiles for ^{124}Xe+^{208}Pb at $E_{\rm c.m.} = 450$ MeV.

a few nucleon transfers between the projectile and target. One can see that the TKEL of the quasi-elastic collision events is less than 30 MeV. The differences between the ImQMD calculations and Gaussian curve are mainly the deep-inelastic collision events. Most of quasi-fission events occur at $400 < t_{\rm con} \leq 1000$ fm/c. The masses distribute in a rather broad range. There are a large number of nucleon transfers, in which may leads to the isospin equilibration between the quasi-projectile and quasi-target fragments.

The average N/Z values of the primary products in ^{58}Ni+^{208}Pb at $E_{\rm lab} = 345$ MeV are shown in Fig. 7. The solid line in Fig. 7(a) denotes the calculations of the ImQMD model with $0 < t_{\rm con} \leq 1000$ fm/c in the region of the impact parameters from 0 to $b_{\rm max}$ fm. The elastic scattering and fusion-fission events are not taken into account. The N/Z values of the projectile, the target, and the compound nucleus are 1.071, 1.537, and 1.418, respectively. From Fig. 7(a), one sees that the experimental data can be reasonably well reproduced by the ImQMD calculations. The average N/Z values of the projectile-like products increase rapidly with increasing nucleon transfer due to the isospin transport from target to projectile. On the curve, a steep valley and a peak can be clearly seen in the vicinity of the projectile and target. This feature was also found in the reactions of ^{64}Ni+^{130}Te and ^{64}Ni+^{208}Pb [18, 43]. In fact,

the isospin equilibration process depends strongly on the contact time of the reaction partners. Figure 7(b) shows the average N/Z values of the primary products with contact time regions of $0 < t_{\rm con} \leq 200$, $200 < t_{\rm con} \leq 400$, and $400 < t_{\rm con} \leq 1000$ fm/c. In case of $0 < t_{\rm con} \leq 200$ fm/c, most of the primary products are produced in the quasi-elastic collisions. The strong neutron flow from the target to projectile results in sharp increase of N/Z values of the projectile-like fragments. However, the system can not reach the situation of complete isospin equilibration due to a short contact time. With increasing contact time, the enhanced effect of the isospin equilibration can be seen clearly. The products of complete isospin equilibration are produced in symmetric quasi-fission reactions. The isospin equilibration process in the MNT reactions can result in the production of very neutron-rich projectile-like fragments. A strong absorption of neutrons by the projectile (^{58}Ni) was observed by the experiment [18]. For example, after neutron evaporation, ^{67}Ni with production cross section about 15 μb has been detected in the $\gamma - \gamma$ coincidence analysis.

IV. CONCLUSIONS

In summary, the production cross sections of isotopes in the reaction of ^{58}Ni+^{208}Pb at $E_{\rm lab} = 328.4$ MeV are calculated by the ImQMD model. The results show that the ImQMD model is suitable to describe the MNT reac-
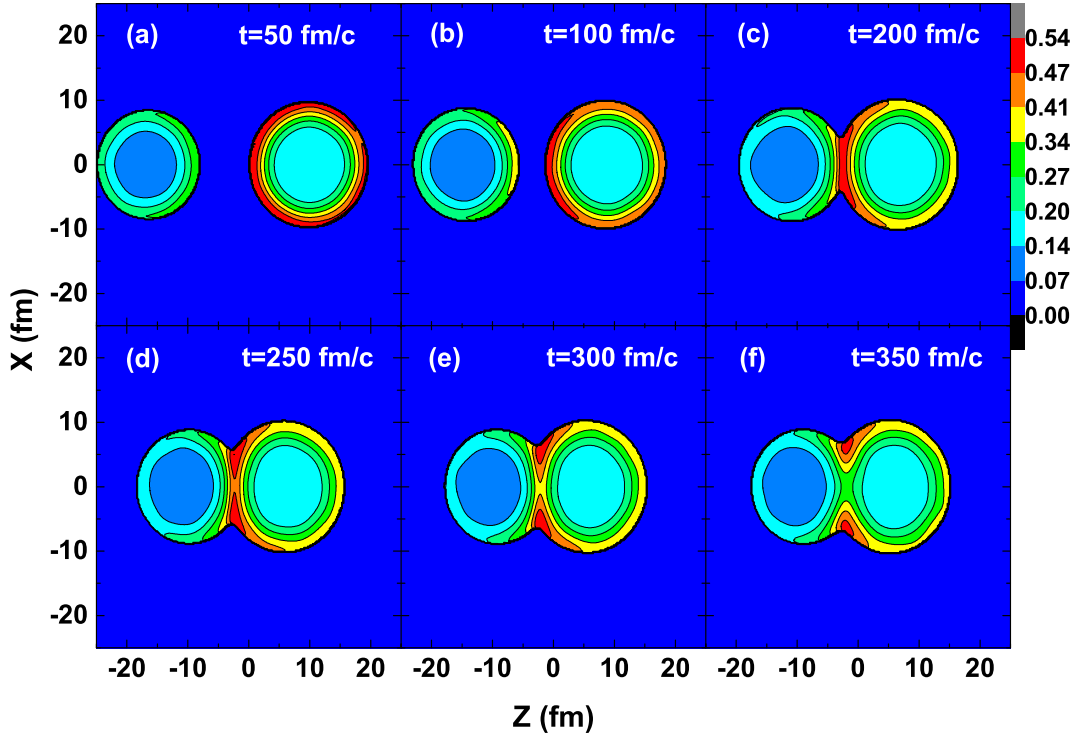
FIG. 4. (Color online.) Time evolution of the isospin asymmetry $\delta = (\rho_n - \rho_p)/(\rho_n + \rho_p)$ distributions for ^{124}Xe+^{208}Pb at $E_{c.m.} = 450$ MeV.

tions at near-barrier energies. The isospin equilibration process in ^{124}Xe+^{208}Pb at head-on collisions is studied. The values of isospin asymmetry in the cores of two reaction partners are uniform during the collisions. The neutrons are preferably driven to the low-density area. On the surface of the nuclei, the value of isospin asymmetry is larger than the core of the nuclei. The direction of neutron flow is from the target to projectile along the low-density path. And the neutrons transfer process is very sensitive to the symmetry energy. The neutron flow is enhanced under the large symmetry energy coefficient. The isospin equilibration process depends strongly on the contact time of the reaction partners. By analysing average N/Z values of the primary binary products in ^{58}Ni+^{208}Pb at $E_{lab} = 345$ MeV, we find that the average N/Z values of the projectile-like products increase rapidly with increasing nucleon transfer. In the quasi-elastic collisions, the system can not reach the situation of complete isospin equilibration due to a short contact time. The complete isospin equilibration process is noticed in symmetric quasi-fission reactions where there are massive transfer of nucleons and large energy dissipation.

[1] M. B. Tsang, T. X. Liu, L. Shi, P. Danielewicz, C. K. Gelbke, X. D. Liu, W. G. Lynch, W. P. Tan, G. Verde, A. Wagner, H. S. Xu, W. A. Friedman, L. Beaulieu, B. Davin, R. T. de Souza, Y. Larochelle, T. Lefort, R. Yanez, V. E. Viola, Jr., R. J. Charity, and L. G. Sobotka, Phys. Rev. Lett. **92**, 062701 (2004).

[2] V. Baran, M. Colonna, M. Di Toro, M. Zielinska-Pfabé, and H. H. Wolter, Phys. Rev. C **72**, 064620 (2005).
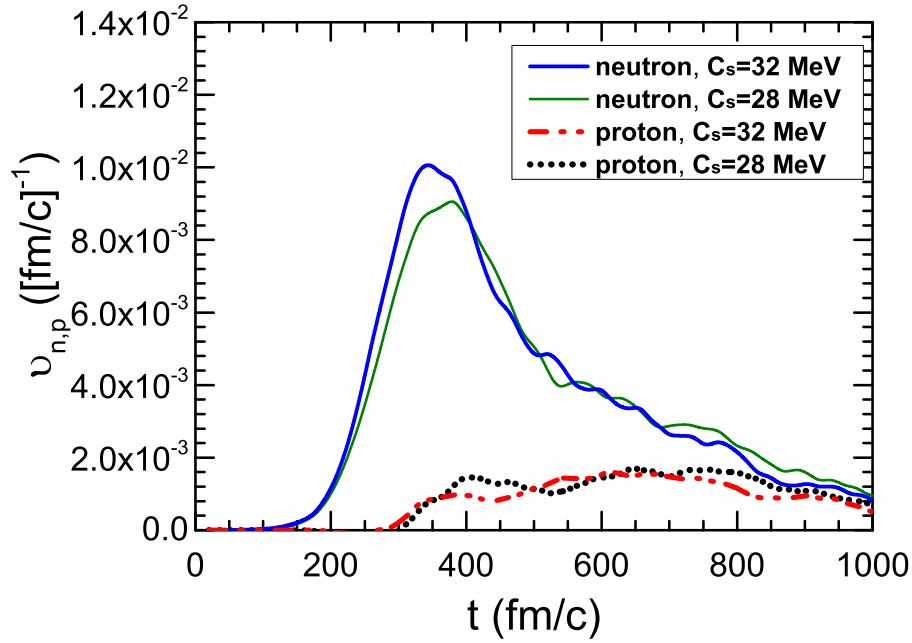
FIG. 5. (Color online.) The transfer coefficients for neutron and proton with symmetry energy coefficients of $C_s = 28$ and 32 MeV in the head-on collisions of ^{124}Xe+^{208}Pb at $E_{c.m.} = 450$ MeV.

[3] I. Lombardo, C. Agodi, R. Alba, F. Amorini, A. Anzalone, I. Berceanu, G. Cardella, S. Cavallaro, M. B. Chatterjee, E. De Filippo, A. Di Pietro, P. Figuera, E. Geraci, G. Giuliani, L. Grassi, A. Grzeszczuk, J. Han, E. La Guidara, G. Lanzalone, N. Le Neindre, C. Maiolino, A. Pagano, M. Papa, S. Pirrone, G. Politi, A. Pop, F. Porto, F. Rizzo, P. Russotto, D. Santonocito, and G. Verde, Phys. Rev. C **82**, 014608 (2010).

[4] D. D. S. Coupland, W. G. Lynch, M. B. Tsang, P. Danielewicz, and Y. X. Zhang, Phys. Rev. C **84**, 054603 (2011).

[5] J. Su, L. Zhu, and C. C. Guo, Phys. Lett. B **782**, 682 (2018).

[6] Z. Y. Sun, M. B. Tsang, W. G. Lynch, G. Verde, F. Amorini, L. Andronenko, M. Andronenko, G. Cardella, M. Chatterje, P. Danielewicz, E. De Filippo, P. Dinh, E. Galichet, E. Geraci, H. Hua, E. La Guidara, G. Lanzalone, H. Liu, F. Lu, S. Lukyanov, C. Maiolino, A. Pagano, S. Piantelli, M. Papa, S. Pirrone, G. Politi, F. Porto, F. Rizzo, P. Russotto, D. Santonocito, and Y. X. Zhang, Phys. Rev. C **82**, 051603(R) (2010).

[7] E. Galichet, M. F. Rivet, B. Borderie, M. Colonna, R. Bougault, A. Chbihi, R. Dayras, D. Durand, J. D. Frankland, D. C. R. Guinet, P. Lautesse, N. Le Neindre, O. Lopez, L. Manduci, M. Parlog, E. Rosato, B. Tamain, E. Vient, C. Volant, and J. P. Wieleczko, Phys. Rev. C **79**, 064614 (2009).

[8] E. Galichet, M. Colonna, B. Borderie, and M. F. Rivet, Phys. Rev. C **79**, 064615 (2009).

[9] S. Barlini, S. Piantelli, G. Casini, P. R. Maurenzig, A. Olmi, M. Bini, S. Carboni, G. Pasquali, G. Poggi, A. A. Stefanini, R. Bougault, E. Bonnet, B. Borderie, A. Chbihi, J. D. Frankland, D. Gruyer, O. Lopez, N. Le

Neindre, M. Pârlog, M. F. Rivet, E. Vient, E. Rosato, G. Spadaccini, M. Vigilante, M. Bruno, T. Marchi, L. Morelli, M. Cinausero, M. Degerlier, F. Gramegna, T. Kozik, T. Twaróg, R. Alba, C. Maiolino, and D. Santonocito, Phys. Rev. C **87**, 054607 (2013).

[10] M. Di Toro, A. Olmi, and R. Roy, Eur.Phys. J. A **30**, 65 (2006).

[11] R. Lionti, V. Baran, M. Colonna, and M. Di Toro, Phys. Lett. B **625**, 33 (2005).

[12] T. Welsh, W. Loveland, R. Yanez, J. S. Barrett, E. A. McCutchan, A. A. Sonzogni, T. Johnson, S. Zhu, J. P. Greene, A. D. Ayangeakaa, M. P. Carpenter, T. Lauritsen, J. L. Harker, W. B. Walters, B. M. S. Amro, and P. Coppe, Phys. Lett. B **771**, 119 (2017).

[13] J. S. Barrett, W. Loveland, R. Yanez, S. Zhu, A. D. Ayangeakaa, M. P. Carpenter, J. P. Greene, R. V. F. Janssens, T. Lauritsen, E. A. McCutchan, A. A. Sonzogni, C. J. Chiara, J. L. Harker, and W. B. Walters, Phys. Rev. C **91**, 064615 (2015).

[14] Y. X. Watanabe, Y. H. Kim, S. C. Jeong, Y. Hirayama, N. Imai, H. Ishiyama, H. S. Jung, H. Miyatake, S. Choi, J. S. Song, E. Clement, G. de France, A. Navin, M. Rejmund, C. Schmitt, G. Pollarolo, L. Corradi, E. Fioretto, D. Montanari, M. Niikura, D. Suzuki, H. Nishibata, and J. Takatsu, Phys. Rev. Lett. **115**, 172503 (2015).

[15] O. Beliuskina, S. Heinz, V. Zagrebaev, V. Comas, C. Heinz, S. Hofmann, R. Knöbel, M. Stahl, D. Ackermann, F. P. Heßberger, B. Kindler, B. Lommel, J. Maurer, and R. Mann, Eur. Phys. J. A **50**, 161 (2014).

[16] V. F. Comas, S. Heinz, S. Hofmann, D. Ackermann, J. A. Heredia, F. P. Heßberger, J. Khuyagbaatar, B. Kindler, B. Lommel, and R. Mann, Eur. Phys. J. A **49**, 112 (2013).
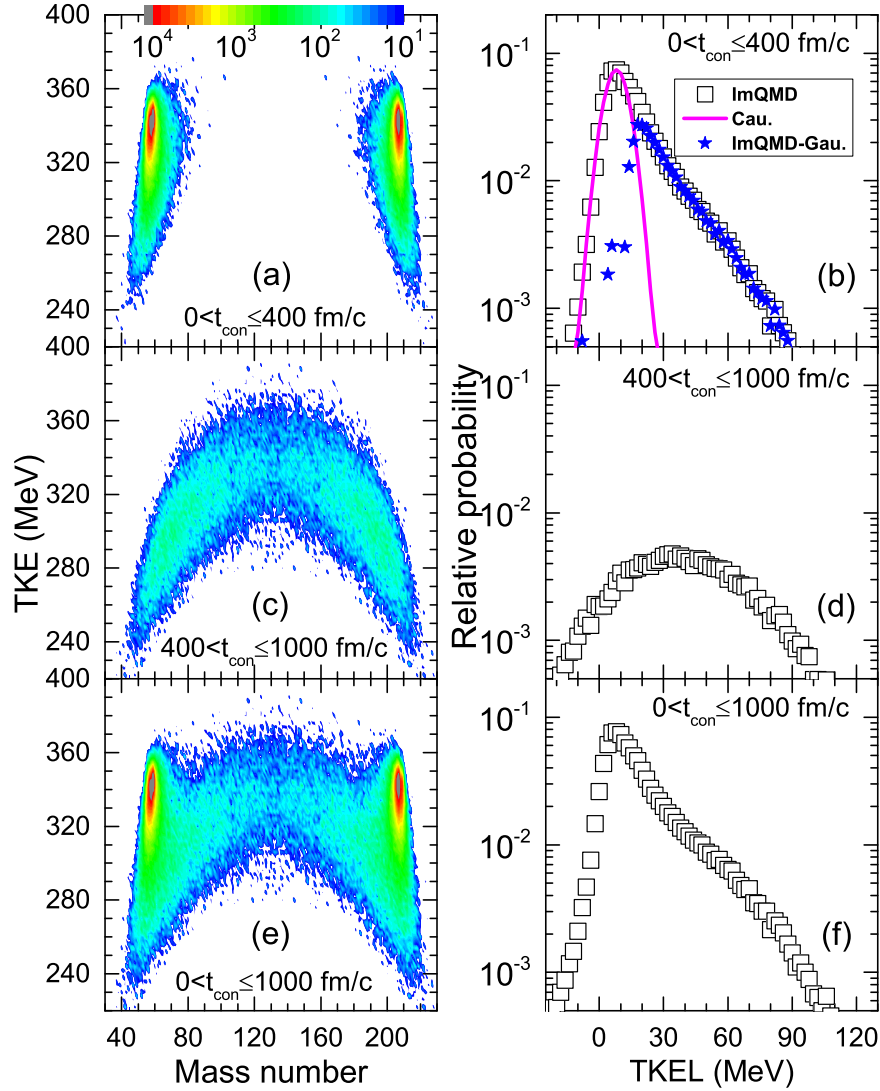
[17] E. M. Kozulin, E. Vardaci, G. N. Knyazheva, A. A. Bo-

FIG. 6. (Color online.) Left panels: TKE-Mass distributions of primary binary fragments for the contact time of $0 < t_{con} \leq 400$, $400 < t_{con} \leq 1000$, and $0 < t_{con} \leq 1000$ fm/c. The right panels are corresponding TKEL distributions. In Fig. 6(b), the solid line is the quasi-elastic (Gaussian-like) contribution; stars are the difference between the ImQMD calculation and the Gaussian distribution.

gachev, S. N. Dmitriev, I. M. Itkis, M. G. Itkis, A. G. Knyazev, T. A. Loktev, K. V. Novikov, E. A. Razinkov, O. V. Rudakov, S. V. Smirnov, W. Trzaska, and V. I. Zagrebaev, Phys. Rev. C **86**, 044611 (2012).

[18] W. Królas, R. Broda, B. Fornal, T. Pawłat, J. Wrzesiński, D. Bazzacco, G. de Angelis, S. Lunardi, R. Menegazzo, D. R. Napoli, and C. Rossi Alvarezb, Nucl. Phys. A **832**, 170 (2010).

[19] A. Vogt, B. Birkenbach, P. Reiter, L. Corradi, T. Mijatović, D. Montanari, S. Szilner, D. Bazzacco, M. Bowry, A. Bracco, B. Bruyneel, F. C. L. Crespi, G. de Angelis, P. Désesquelles, J. Eberth, E. Farnea, E. Fioretto, A. Gadea, K. Geibel, A. Gengelbach, A. Giaz, A. Görgen, A. Gottardo, J. Grebosz, H. Hess, P. R. John, J. Jolie,

D. S. Judson, A. Jungclaus, W. Korten, S. Leoni, S. Lunardi, R. Menegazzo, D. Mengoni, C. Michelagnoli, G. Montagnoli, D. Napoli, L. Pellegri, G. Pollarolo, A. Pullia, B. Quintana, F. Radeck, F. Recchia, D. Rosso, E. Şahin, M.D. Salsac, F. Scarlassara, P.-A. Söderström, A.M. Stefanini, T. Steinbach, O. Stezowski, B. Szpak, Ch. Theisen, C. Ur, J. J. Valiente-Dobón, V. Vandone, and A. Wiens, Phys. Rev. C **92**, 024619 (2015).

[20] T. Mijatović, S. Szilner, L. Corradi, D. Montanari, G. Pollarolo, E. Fioretto, A. Gadea, A. Goasduff, D. J. Malenica, N. Mărginean, M. Milin, G. Montagnoli, F. Scarlassara, N. Soić, A. M. Stefanini, C. A. Ur, and J. J. Valiente-Dobón, Phys. Rev. C **94**, 064616 (2016).
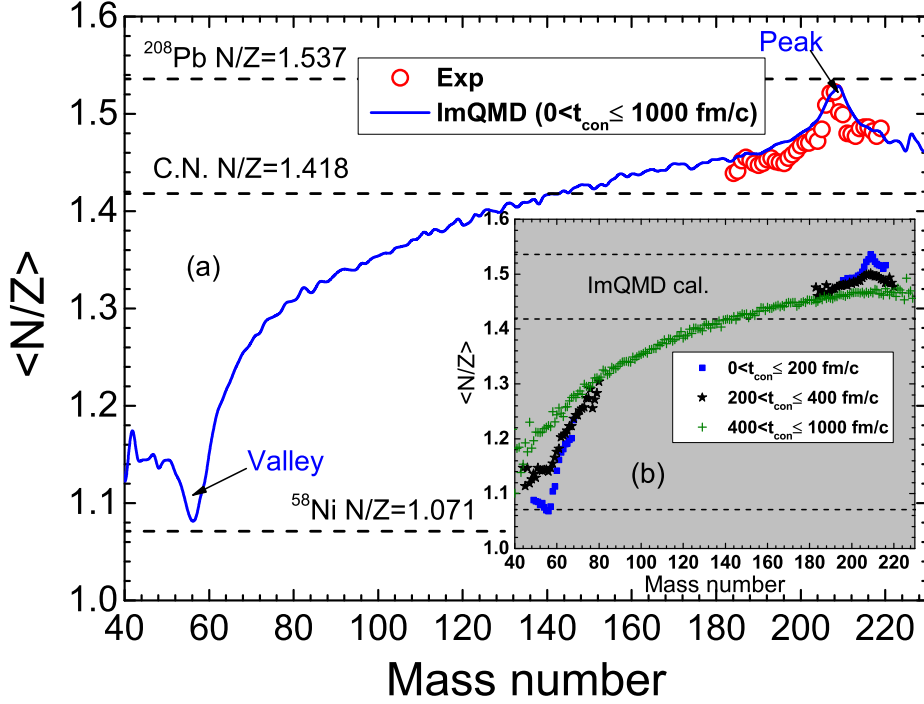
[21] M. V. Pajtler, S. Szilner, L. Corradi, G. de Angelis,

FIG. 7. (Color online.) (a) Average N/Z values for primary binary products of ^{58}Ni+^{208}Pb at $E_{\mathrm{lab}} = 345$ MeV. The solid line denotes the calculations of the ImQMD model with $0 < t_{con} \leq 1000$ fm/c. The dashed lines indicate the N/Z values of the projectile, the target, and the compound nucleus. The elastic scattering and fusion-fission events are not included. The experimental data (open circles) are reconstructed primary fragments taken from Ref. [18]. (b) Calculated average N/Z values of the primary binary products with contact time of $0 < t_{con} \leq 200$, $200 < t_{con} \leq 400$, and $400 < t_{con} \leq 1000$ fm/c.

E. Fioretto, A. Gadea, F. Haas, S. Lunardi, D.Jelavić Malenica, N. Mărginean, D. Mengoni, T. Mijatović, G. Montagnoli, D. Montanari, G. Pollarolo, F. Recchia, M.-D. Salsac, F. Scarlassara, N. Soić, A.M. Stefanini, C. A. Ur, and J. J. Valiente-Dobón, Nucl. Phys. A **941**, 273 (2015).

[22] L. Corradi, G. Pollarolo, and S. Szilner, J. Phys. G **36**, 113101 (2009).

[23] V. I. Zagrebaev and W. Greiner, Phys. Rev. Lett. **101**, 122701 (2008).

[24] C. Li, P. W. Wen, J. J. Li, G. Zhang, B. Li, X. X. Xu, Z. Liu, S. Zhu, and F. S. Zhang, Phys. Lett. B **776**, 278 (2018).

[25] C. Li, P. W. Wen, J. J. Li, G. Zhang, B. Li, and F. S. Zhang, Nucl. Sci. Tech. **28**, 110 (2017).

[26] H. Yao and N. Wang, Phys. Rev. C **95**, 014607 (2017).

[27] N. Wang and L. Guo, Phys. Lett. B **760**, 236 (2016).

[28] L. Zhu, J. Su, W.J. Xie, and F.S. Zhang, Phys. Lett. B **767**, 437 (2017).

[29] L. Zhu, P. W. Wen, C. J. Lin, X. J. Bao, J. Su, C. Li, and C. C. Guo, Phys. Rev. C **97**, 044614 (2018).

[30] Z. Q. Feng, Phys. Rev. C **95**, 024615 (2017).

[31] K. Zhao, Z. X. Li, Y. X. Zhang, N. Wang, Q. F. Li, C. W. Shen, Y. J. Wang, and X. Z. Wu, Phys. Rev. C **94**, 024601 (2016).

[32] C. Li, F. Zhang, J. J. Li, L. Zhu, J. L. Tian, N. Wang, and F.S. Zhang, Phys. Rev. C **93**, 014618 (2016).

[33] M. Veselsky and G. A. Souliotis, Nucl. Phys. A **872**, 1

(2011).

[34] G. G. Adamian, N. V. Antonenko, V. V. Sargsyan, and W. Scheid, Phys. Rev. C **81**, 057602 (2010).

[35] Yu. E. Penionzhkevich, G. G. Adamian, and N. V. Antonenko, Phys. Lett. B **621**, 119 (2005).

[36] E. M. Kozulin, G. N. Knyazheva, S. N. Dmitriev, I. M . I tkis, M. G. Itkis, T. A.Loktev, K. V. Novikov, A. N. Baranov, W. H. Trzaska, E. Vardaci, S. Heinz, O. Beliuskina, and S. V. Khlebnikov, Phys. Rev. C **89**, 014614 (2014).

[37] E. M. Kozulin, V. I. Zagrebaev, G. N. Knyazheva, I. M. Itkis, K. V. Novikov, M. G. Itkis, S. N. Dmitriev, I. M. Harca, A. E. Bondarchenko, A. V. Karpov, V. V. Saiko, and E. Vardaci, Phys. Rev. C **96**, 064621 (2017).

[38] G. N. Knyazheva, E. M. Kozulin, R. N. Sagaidak, A. Yu. Chizhov, M. G. Itkis, N. A. Kondratiev, V. M. Voskressensky, A. M. Stefanini, B. R. Behera, L. Corradi, E. Fioretto, A. Gadea, A. Latina, S. Szilner, M. Trotta, S. Beghini, G. Montagnoli, F. Scarlassara, F. Haas, N. Rowley, P. R. S. Gomes, and A. Szanto de Toledo, Phys. Rev. C **75**, 064602 (2007).

[39] R. du Rietz, D. J. Hinde, M. Dasgupta, R. G. Thomas, L. R. Gasques, M. Evers, N. Lobanov, and A. Wakhle, Phys. Rev. Lett. **106**, 052701 (2011).

[40] E. Prasad, D. J. Hinde, E. Williams, M. Dasgupta, I. P. Carter, K. J. Cook, D. Y. Jeung, D. H. Luong, C. S. Palshetkar, D. C. Rafferty, K. Ramachandran, C. Simenel, and A. Wakhle, Phys. Rev. C **96**, 034608 (2017).

[41] R. T. de Souza, W. U. Schröder, J. R. Huizenga, R. Planeta, K. Kwiatkowski, V. E. Viola, and H. Breuer, Phys. Rev. C **37**, 1783(R) (1988).

[42] R. Planeta, S. H. Zhou, K. Kwiatkowski, W. G. Wilson, V. E. Viola, H. Breuer, D. Benton, F. Khazaie, R. J. McDonald, A. C. Mignerey, A. Weston-Dawkes, R. T. de Souza, J. R. Huizenga, and W. U. Schröder, Phys. Rev. C **38**, 195 (1988).

[43] W. Królas, R. Broda, B. Fornal, T. Pawłat, H. Grawe, K. H. Maier, M. Schramm, and R. Schubart, Nucl. Phys. A **724**, 289 (2003).

[44] D. Guerreau, J. Galin, B. Gatty, and X. Tarrago, Z. Phys. A **295**, 105 (1980).

[45] N. Wang, Z. X. Li, and X. Z. Wu, Phys. Rev. C **65**, 064608 (2002).

[46] N. Wang, Z. X. Li, X. Z. Wu, J. L. Tian, Y. X. Zhang, and M. Liu, Phys. Rev. C **69**, 034608 (2004).

[47] J. Aichelin, Phys. Rep. **202**, 233 (1991).

[48] M. Papa, T. Maruyama, and A. Bonasera, Phys. Rev. C **64**, 024612 (2001).

[49] G. Giuliani, H. Zheng, and A. Bonasera, Prog. Part. Nulc. Phys. **76**, 116 (2014).

[50] N. Wang, L. Ou, Y. X. Zhang, and Z. X. Li, Phys. Rev. C **89**, 064601 (2014).

[51] J. L. Tian, X. Z. Wu, K. Zhao, Y. X. Zhang, and Z. X. Li, Phys. Rev. C **77**, 064603 (2008).

[52] L. Corradi, A. M. Vinodkumar, A. M. Stefanini, E. Fioretto, G. Prete, S. Beghini, G. Montagnoli, F. Scarlassara, G. Pollarolo, F. Cerutti, and A. Winther, Phys. Rev. C **66**, 024606 (2002).

[53] A. Winther, Nucl. Phys. A **572**, 191 (1994).

[54] A. Winther, Nucl. Phys. A **594**, 203 (1995).

[55] http://personalpag es.to.infn.it/~nanni/grazing/.

[56] R. J. Charity, Phys. Rev. C **82**, 014610 (2010).

[57] R. Lionti, V. Baran, M. Colonna, and M. Di Toro, Phys. Lett. B **625**, 33 (2005).

[58] K. Washiyama and D. Lacroix, Phys. Rev. C **78**, 024610 (2008).

[59] S. Ayik, K. Washiyama, and D. Lacroix, Phys. Rev. C **79**, 054606 (2009).

[60] S. Ayik, B. Yilmaz, and O. Yilmaz, Phys. Rev. C **92**, 064615 (2015).